American Mineralogist, Volume 84, pages 477–492, 1999

Modeling of the solubility of a two-component $H_2O + CO_2$ fluid in silicate liquids

PAOLO PAPALE*

CNR-GNV, Centro di Studio per la Geologia Strutturale e Dinamica dell'Appennino, Via S. Maria 53, 56126 Pisa, Italy

ABSTRACT

The solubility of a two-component, $H_2O + CO_2$ fluid in silicate liquids was modeled by assuming mechanical, thermal, and chemical equilibrium between the fluid and liquid phases. The liquid phase was treated as a 12-component (10 major oxides + H_2O + CO_2) mixture, and its thermodynamic properties were calculated on the basis of a regular and non-isometric mixing equation for the excess Gibbs free energy. The mole fractions of the exsolved and dissolved water and carbon dioxide were calculated on the basis of two chemical equilibrium and two mass-balance equations expressing the conservation of the exsolved and total mass of volatiles. The model was then calibrated by processing nearly 1000 experimental H_2O and CO_2 solubility determinations from the literature in natural and synthetic silicate liquids covering a wide range of pressure-temperature-composition conditions. The results show that the present model predicts with reasonable accuracy the solubility of water and carbon dioxide in silicate liquids over the entire range of fluid phase compositions and for pressures from atmospheric to several hundreds of megapascals and temperatures from about 1000 to 1900 K. The predicted isobaric-isothermal sections of the $H_2O + CO_2$ saturation surface show a transition from essentially Henrian to strongly non-Henrian behavior as the pressure is increased from tens to hundreds of megapascals, consistent with the majority of experimental results made at low, medium, and high pressure. The presence of a very small amount of CO_2 in the system significantly increases the volatile saturation pressure, suggesting that in most cases the multicomponent nature of the fluid phase cannot be neglected when modeling volcanic processes such as magma chamber and conduit ascent dynamics. The predicted closed- and open-system saturation conditions differ significantly. Under open-system conditions, the dissolved H_2O content increases and the dissolved CO_2 content decreases compared with the closed-system conditions. This results in a more efficient H_2O enrichment of the fluid phase with decreasing pressure under open-system conditions. The present model can be used to investigate the behavior of volatiles in the volcanic environment provided that the basic assumption of equilibrium is satisfied.

INTRODUCTION

It has long been recognized that volcanic gases play a fundamental role in almost all volcanic processes from the deep regions of magma segregation to the eruptions at the surface (Tuttle and Bowen 1958; Hamilton et al. 1964; Tait et al. 1989; Papale et al. 1998). The modeling of the solubility of volcanic gases in liquid magma is fundamental to the understanding of the chemical and physical processes that a magma body undergoes throughout its history, thus for the modeling of most volcanic processes. In a previous paper (Papale 1997), the saturation of H_2O and CO_2 in silicate liquids was modeled in the case where only one of the two volatiles is present in the system. By employing an expression for the reference state of each dissolved volatile and an equation for the excess Gibbs free energy of the liquid mixture, and by processing more than 900 experimental H_2O and CO_2 solubility determinations from the literature covering a wide range of pressure, temperature, and composition conditions, it was found that the H_2O solubility data are well reproduced by a regular and isometric mixing equation for the liquid phase, whereas the CO_2 solubility data agree better with a regular and non-isometric form of the mixing equation, implying that the binary interaction coefficients involving CO_2 are pressure dependent. The characteristics of the saturation surface of each volatile that are reproduced by such modeling include the change from retrograde to prograde water solubility with increasing temperature in albitic liquids (Paillat et al. 1992), the alkali effect of H_2O (Holtz et al. 1995), the increasing CO_2 solubility with increasing degree of silica undersaturation (Mysen et al. 1975; Dixon 1997), the Henrian behavior of CO_2 in most silicate liquids up to 30–50 MPa (Dixon et al. 1995), and the linear relationship between the fugacity in the fluid phase or the activity in the liquid phase and the square of the mole fraction of the dissolved

* E-mail: papale@dst.unipi.it

0003–004X/99/0004–0477$05.00

volatile at saturation shown by some unrelated silicate liquid compositions (McMillan 1994).

The present paper extends the modeling of the solubility of H_2O and CO_2 in silicate liquids by considering the more realistic case in which the two volatiles are present simultaneously in the system. The objective is different from that of previously published simpler models (Gerlach 1986; Holloway and Blank 1994; Dixon and Stolper 1995; Dixon et al. 1995; Dixon 1997), which were designed to reproduce accurately a subset of the experimental H_2O-CO_2 saturation data within a narrow range of pressure-temperature-liquid composition. In contrast, the present model is designed to work in the entire *P-T*-composition range defined by the majority of experimental data. This requires a more comprehensive theoretical formulation because the objective of the model prevents the calibration of quantities that are nearly constant in a restricted range of conditions but may vary widely when the conditions vary significantly.

The new model is then used to predict the combined H_2O-CO_2 saturation surface in several liquids of different composition, and such predictions are compared with the available experimental data. It will be shown that the model correctly predicts a mutual effect of H_2O and CO_2 in reducing their saturation content up to pressures of several hundred megapascals, as well as an essentially Henrian behavior of the two volatiles in the liquid phase at low and constant pressure, and significant deviations from such behavior at pressures above 0.1 GPa.

Description of the model

In this paper, it is assumed that the fluid phase coexisting with a silicate liquid contains H_2O and CO_2 as the only components, and that the liquid and fluid phases are in thermodynamic equilibrium. Under these conditions, the equations describing the mechanical, thermal, and chemical equilibrium are:

$$P^{G} = P^{L} = P \tag{1}$$

$$T^{G} = T^{L} = T \tag{2}$$

$$f^{G}_{H_2O} = f^{L}_{H_2O} \tag{3}$$

$$f^{G}_{CO_2} = f^{L}_{CO_2} \tag{4}$$

where P is pressure, T is temperature, f is fugacity, and the superscripts G and L refer to the fluid and liquid phase, respectively. By employing the first two equations and introducing the fugacity coefficient in the fluid phase ϕ, activity coefficient in the liquid phase γ, and reference state fugacity f^0, Equations 3 and 4 become:

$$\phi_{H_2O} y_{H_2O} P = \gamma_{H_2O} x_{H_2O} f^{0L}_{H_2O} \tag{5}$$

$$\phi_{CO_2} y_{CO_2} P = \gamma_{CO_2} x_{CO_2} f^{0L}_{CO_2} \tag{6}$$

where y and x are the mole fractions in the fluid and liquid phase, respectively. No account is taken of the true form, molecular or dissociated, of the dissolved volatiles (this point is extensively discussed in Papale 1997). Equations 5 and 6 are the basic expressions describing the equilibrium between the liquid and fluid phases. These are closed by two mass-balance equations describing the conservation of the exsolved and total gas, respectively:

$$y_{H_2O} + y_{CO_2} = 1 \tag{7}$$

$$\frac{x^{T}_{H_2O} - x_{H_2O}}{y_{H_2O} - x_{H_2O}} = \frac{x^{T}_{CO_2} - x_{CO_2}}{y_{CO_2} - x_{CO_2}} \tag{8}$$

where the superscript T refers to the total mole fraction of each volatile. The system formed by Equations 5–8 can be solved for x_{H2O}, x_{CO_2}, y_{H_2O}, and y_{CO_2}, for any given $x^{T}_{H_2O}$ and $x^{T}_{CO_2}$, provided that expressions for ϕ_{H_2O}, ϕ_{CO_2}, γ_{H_2O}, γ_{CO_2}, $f^{0L}_{H_2O}$, and $f^{0L}_{CO_2}$, are known. A modified Redlich-Kwong equation of state for pure H_2O, pure CO_2, and H_2O-CO_2 mixtures (Kerrick and Jacobs 1981) is used to describe the properties of the fluid phase. An expression for f^{0L}_i (where the component i is either H_2O or CO_2) is given in Papale (1997), and it requires the definition of an equation of state for the reference molar volume v_i of the dissolved volatile in the liquid phase:

$$RT \ln f^{0L}_i = RT \ln f^{0L}_i(P^0_i, T^0_i) + \int_{P^0_i}^{P} v_i \, dP - T \int_{T^0_i}^{T} \frac{1}{T^2} \int_{P^0_i}^{P} \left[v_i - T\left(\frac{\partial v_i}{\partial T}\right)_P \right] dP \, dT \tag{9}$$

where R is the gas constant. The reference molar volumes v_{H_2O} and v_{CO_2} are expressed as a polynomial of the following form:

$$v_i = a_1 + a_2 T + a_3 T^2 + a_4 T^3 + P(a_5 + a_6 T + a_7 T^2) + P^2(a_8 + a_9 T) + a_{10} P^3. \tag{10}$$

The activity coefficients γ_{H_2O} and γ_{CO_2} can be obtained by the relation:

$$RT \ln \gamma_i = \left(\frac{\partial G^E}{\partial n_i}\right)_{P,T,n_{j \neq i}} \tag{11}$$

where G^E is the excess Gibbs free energy of the liquid mixture, and n_i and n_j denote the number of moles of component i and j. The excess Gibbs free energy G^E is expressed as:

$$G^E = \frac{1}{2} N \sum_{i=1}^{m} \sum_{j=1}^{m} x_i x_j w_{ij} \tag{12}$$

where N is the total number of moles in the liquid phase, m is the total number of components in the liquid phase (12, made up of 2 volatiles + 10 major oxides), and w_{ij} are symmetric binary interaction coefficients ($w_{ij} = w_{ji}$; $w_{ii} = 0$) describing the attractive-repulsive behavior of each pair of components. It was found previously (Papale 1997) that the H_2O and CO_2 solubility data in the one-component fluid phase condition are reproduced with reasonable accuracy by using the following relations:

$$w_{H_2Oj} = w^{(0)}_{H_2Oj} \tag{13}$$

$$w_{CO_2 j} = w^{(0)}_{CO_2 j} + \ln\frac{P}{P^0} w^{(1)}_{CO_2 j} \tag{14}$$

where the $w^{(0)}_{ij}$ ($i = H_2O$, CO_2) and $w^{(1)}_{CO_2 j}$ terms are calibrated by robust weighted linear least-squares regression (Press et al. 1992), and the w_{ij} ($i,j \neq H_2O$, CO_2) terms are taken from Ghiorso et al. (1983). The implications of the different functional form of the interaction coefficients involving H_2O and CO_2 and their consistency with the mechanisms of H_2O and CO_2 dissolution on a molecular scale are discussed in Papale (1997). By extending this approach to the two-component fluid phase condition, and by rewriting the mole fractions in the liquid phase with the following specification:

$$x'_{i\neq H_2O,CO_2} = \frac{x_i}{1 - x_{H_2O} - x_{CO_2}} \tag{15}$$

the resulting expressions for γ_{H_2O} and γ_{CO_2} are:

$$\begin{aligned} RT \ln \gamma_{H_2O} = {} & (1 - x_{H_2O}) x_{CO_2} w_{H_2OCO_2} \\ & + (1 - x_{H_2O})(1 - x_{H_2O} - x_{CO_2}) \sum_{\substack{i=1 \\ i\neq CO_2}}^{n} x'_i w^{(0)}_{H_2Oi} \\ & - x_{CO_2}(1 - x_{H_2O} - x_{CO_2}) \\ & \times \left[\sum_{\substack{i=1 \\ i\neq H_2O}}^{n} x'_i w^{(0)}_{CO_2 i} + \ln\frac{P}{P^0} \sum_{\substack{i=1 \\ i\neq H_2O}}^{n} x'_i w^{(1)}_{CO_2 i} \right] \\ & - (1 - x_{H_2O} - x_{CO_2})^2 \sum_{\substack{i=1 \\ i\neq H_2O,CO_2}}^{n-1} \sum_{\substack{j=i+1 \\ j\neq H_2O,CO_2}}^{n} x'_i x'_j w_{ij} \end{aligned} \tag{16}$$

$$\begin{aligned} RT \ln \gamma_{CO_2} = {} & (1 - x_{CO_2}) x_{H_2O} w_{H_2OCO_2} \\ & - x_{H_2O}(1 - x_{H_2O} - x_{CO_2}) \sum_{\substack{i=1 \\ i\neq CO_2}}^{n} x'_i w^{(0)}_{H_2Oi} \\ & + (1 - x_{CO_2})(1 - x_{H_2O} - x_{CO_2}) \\ & \times \left[\sum_{\substack{i=1 \\ i\neq H_2O}}^{n} x'_i w^{(0)}_{CO_2 i} + \ln\frac{P}{P^0} \sum_{\substack{i=1 \\ i\neq H_2O}}^{n} x'_i w^{(1)}_{CO_2 i} \right] \\ & - (1 - x_{H_2O} - x_{CO_2})^2 \sum_{\substack{i=1 \\ i\neq H_2O,CO_2}}^{n-1} \sum_{\substack{j=i+1 \\ j\neq H_2O,CO_2}}^{n} x'_i x'_j w_{ij} \end{aligned} \tag{17}$$

where $w_{H_2O\text{-}CO_2}$ is an H_2O-CO_2 interaction coefficient whose form (if constant or *P-T* dependent) is not defined for the moment. A significant difference between the one- and two-component fluid phase conditions is that the presence of a component, CO_2, with non-isometric mixing with the silicate liquid produces a *P*-dependence of the activity coefficient of H_2O even if the employed $w_{H_2O\text{-}i}$ coefficients are not pressure dependent. Another significant difference is that the amount of each volatile dissolved in the liquid is not determined uniquely by specifying the *P-T*-composition conditions (as in the case of a pure H_2O or pure CO_2 fluid phase), but also depends on the total amounts of H_2O and CO_2 in the system (Eq. 8).

The system of Equations 5–8, with the specifications given in Equations 9, 10, 16, and 17, can be solved numerically for any fluid phase composition in terms of H_2O and CO_2. The system can be reduced to two non-linear equations, which can be solved by employing a globally convergent generalized Newton method with backtracking of the iteration step (Press et al. 1992). It is easy to verify that if one of the two volatiles, H_2O and CO_2, is absent from the system, the model presented here reduces to the one-component fluid phase model presented in Papale (1997). This implies that, apart from the H_2O-CO_2 interaction coefficient $w_{H_2O\text{-}CO_2}$ in Equations 16 and 17 and provided that the model is correctly formulated, the model parameters can be obtained entirely from the regression of the pure H_2O and pure CO_2 solubility data in Papale (1997). This is an important point, since (1) it allows a proper model calibration even if the two-component saturation data are scarce and (2) it allows a very significant check of the model formulation by predicting the two-component fluid phase saturation surface on the basis of the one-component solubility data. Note that the latter point does not imply that the present model is a sort of superposition of the results pertaining to the pure volatile solubility data, because the activity coefficient of each dissolved volatile is described in terms of the liquid composition including the other dissolved volatile. It is shown below that this allows an extension of the model predictions far above the limiting conditions of the to-date simpler models, up to the high-pressure field where complex (non-Henrian) behavior is found experimentally.

In the following section a re-derivation of the CO_2-related model parameters is presented. This re-derivation is made to account for the well-known large internal inconsistencies shown by the pure CO_2 solubility data, and represents a correction to the CO_2-related model parameters calibrated previously (Papale 1997).

RE-DERIVATION OF THE CARBON DIOXIDE-RELATED MODEL PARAMETERS

It is well-known (Blank and Brooker 1994; Holloway and Blank 1994) that one of the major challenges in understanding the mechanisms of CO_2 solubility in silicate liquids is represented by the large inconsistencies shown by the CO_2 solubility data produced by the different authors with different experimental techniques. Indeed, differences by a factor of several units can be found in the literature for very similar experimental conditions. In particular, the data of Mysen and co-workers (Mysen 1976; Mysen et al. 1974, 1975, 1976; Holloway et al. 1976; Eggler and Mysen 1976; Mysen and Virgo 1980a, 1980b) have been criticized by many authors (see for example Stolper et al. 1987; Lange 1994) as having low accuracy because of the ^{14}C β-track mapping technique used in the

determination of the CO_2 content of the quenched glass. Unfortunately, these data constitute a considerable part of the existing experimental determinations of CO_2 solubility in silicate liquids, and represent >60% of the data employed in the database for the extraction of the CO_2 solubility model parameters in Papale (1997). As a consequence of such large inconsistencies among the data, the comparison between the experimental results and the model predictions (see Fig. 5 of Papale 1997) shows a large scattering and the employed robust estimate technique produces outlying points (i.e., data points that are automatically excluded by the regression as lying far from the fit of the main body of data), which include many recent experimental determinations whose accuracy is generally considered high. This problem is addressed in Papale (1997), where an attempt was made to re-derive the CO_2 model parameters by excluding all the data produced before the 1980s (see the Appendix). Unfortunately, such an attempt was not successful because the few remaining data points (94) did not allow the extraction of stable model parameters, and the model failed to predict reasonable CO_2 solubilities for silicate liquid compositions different from those used in the regression. For this reason Papale (1997) decided to retain all the data in the database, and to accept the poor agreement between some of them and the corresponding model predictions as a limit imposed by the lack of consistency among the experimental determinations.

In the present paper, the extension of the modeling to the two-component H_2O + CO_2 fluid phase conditions allows the inclusion in the database of many recent experimental data [seven from Blank et al. (1993) and six from Dixon et al. (1995)], producing 26 additional lines in the design matrix (each experimental determination of H_2O + CO_2 solubility produces two equilibrium equations, one for H_2O and one for CO_2; Eqs. 5 and 6). The recent data of Jacobsson (1997) on the H_2O + CO_2 saturation in an icelanditic melt at P = 1 GPa and T = 1673 K are not included in the database, because at this high pressure the uncertainty in the predicted amount of dissolved H_2O is large (Papale 1997) and results in a poor constraint on the CO_2-related model parameters. The data produced before the 1980s are included in the database for the regression of the CO_2 model parameters but they are processed in a different way, by arbitrarily increasing the associated experimental uncertainties by one order of magnitude (after having verified that by increasing them by more than a factor of 10 does not change the model predictions significantly). The total number of lines in the design matrix (i.e., the total number of independent observations used to constrain the model parameters) is 289, produced by 263 CO_2 and 13 H_2O + CO_2 saturation determinations.

By itself, the scarcity of data on the H_2O + CO_2 fluid saturation in silicate liquids is not a major limit on the regression procedure. Such data are absolutely necessary only to evaluate one model parameter, i.e., the cross-volatile interaction coefficient $w_{H_2O\text{-}CO_2}$ in Equations 16 and 17. If the model is formulated correctly, its theoretical framework allows the calibration of all the other model parameters based on only the pure H_2O and pure CO_2 solubility data. In contrast, the H_2O + CO_2 saturation experiments are fundamental to evaluate the model predictions. If the model is able to reproduce the main features of the saturation surface in one- and two-component fluid phase conditions by comparison with the existing data and with the predictions of other simpler models working in restricted regions of the P-T-composition space, then we can conclude that the theoretical framework of the model captures the relevant physics of fluid-liquid equilibrium and the objective of the model is achieved.

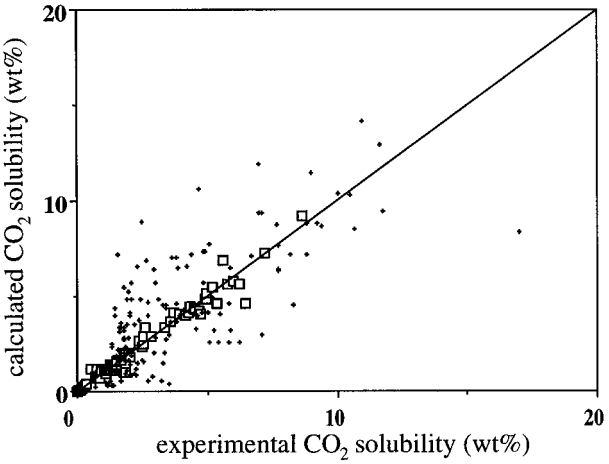

FIGURE 1. Comparison between the experimental and calculated CO_2 solubilities for all the CO_2 solubility data used in the regression. Group 1 data (94 points) are represented as squares, and group 2 data (169 points) as small crosses. Group 1 data: Rai et al. (1983) (6); Stolper et al. (1987) (18); Stolper and Holloway (1988) (5); Mattey et al. (1990) (11); Fogel and Rutherford (1990) (18); Pan et al. (1991) (15); Pawley et al. (1992) (5); Thibault and Holloway (1994) (16). Group 2 data: Mysen et al. (1974) (7); Brey and Green (1975) (1); Mysen et al. (1975) (16); Mysen (1976) (41); Mysen et al. (1976) (33); Eggler and Mysen (1976) (4); Holloway et al. (1976) (17); Brey (1976) (15); Brey and Green (1976) (5); Mysen and Virgo (1980a) (16); Mysen and Virgo (1980b) (14).

The details of the robust estimate technique employed for the regression are illustrated in Appendix 1, and a synthetic description of the database is reported in Appendix 2.

RESULTS

Carbon dioxide

Figure 1 compares calculated and experimental solubilities for all the data used in the regression. The data are divided into two groups: group 1 (squares), which includes the recent experimental determinations; and group 2 (small crosses), which includes data produced before the 1980s. Most of the group 1 data are reproduced within 15% of accuracy, whereas the group 2 data are highly dispersed. It is worth noting that in those cases

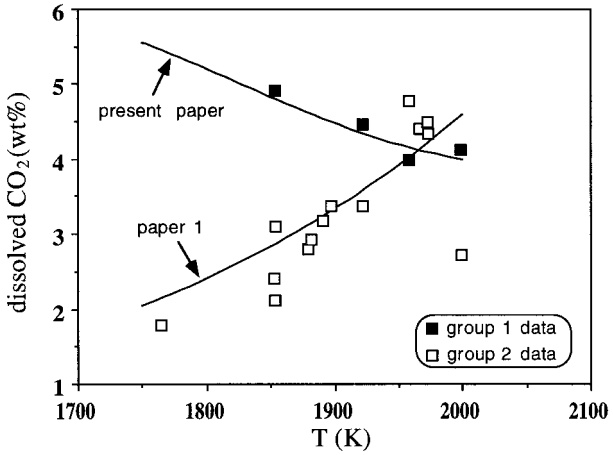

FIGURE 2. Comparison between the experimental group 1 (filled symbols) and group 2 (open symbols) data and the model predictions from Papale (1997) and from the present paper (lines) on the CO_2 solubility in a diopsidic liquid at 2 GPa as a function of temperature. Group 1 data from Rai et al. (1983). Group 2 data from Mysen et al. (1974), Mysen et al. (1976), Holloway et al. (1976), and Mysen and Virgo (1980a, 1980b). See text for discussion.

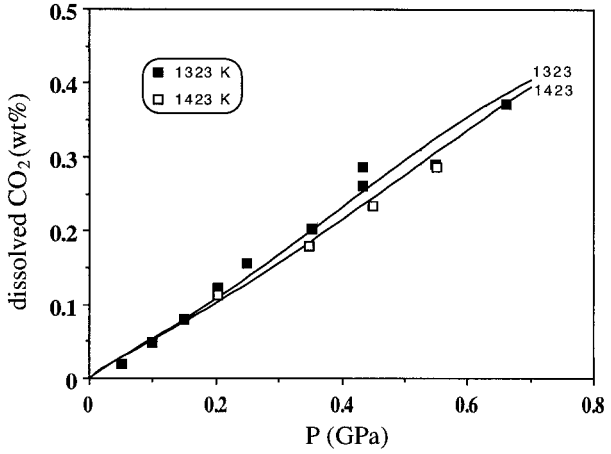

FIGURE 3. Comparison between the experimental (symbols) and calculated (lines) CO_2 solubility in a rhyolitic liquid as a function of pressure at two different temperatures of 1323 and 1423 K. Experimental data and liquid compositions from Fogel and Rutherford (1990).

where the experimental conditions allow a direct comparison, the group 1 and group 2 data are highly inconsistent. This is well illustrated by the example of Figure 2 for liquids of diopsidic composition and $P = 2$ GPa. The model predictions obtained by using the model parameters from Papale (1997) and those from the present paper are also shown on this figure. It can be seen that the group 1 data produce a negative T-dependence of the CO_2 solubility, whereas the group 2 data show a strong positive T-dependence and significant internal disagreement at both low and high temperatures. The use of the model parameters from Papale (1997) produces a substantial agreement with the ^{14}C β-track determinations that dominate the database, whereas the present parameters produce CO_2 solubilities that agree well with the more recent determinations from Rai et al. (1983) based on high-temperature mass spectrometry.

Figure 3 compares the model predictions with the experimental data from Fogel and Rutherford (1990) on the CO_2 solubility in a rhyolitic liquid as a function of pressure at temperatures of 1323 and 1423 K. The agreement is fairly good, and both the model and the data produce a slight negative T-dependence for the dissolution of CO_2.

In Figure 4, the predicted T-dependence for the dissolution of CO_2 in silicate liquids of leucititic and tholeiitic composition at pressures from 0.1 to 2 GPa is compared with the experimental data from Pan et al. (1991) and Thibault and Holloway (1994). The agreement is good, and the experimental CO_2 data are well reproduced by the model in a wide range of P-T conditions. Both the data and the model produce a larger CO_2 solubility in leucititic than in tholeiitic liquids at equal P-T conditions, an essentially null effect of temperature in tholeiitic liquids up to 1.5 GPa pressure, and a progressively increasing negative dependence on temperature with increasing pressure in leucititic liquid.

To verify the stability of the model predictions over a wide compositional range, Figure 5 illustrates calculated CO_2 solubilities in several liquid compositions different from those considered in the database. The model correctly predicts larger CO_2 solubilities for more SiO_2-undersaturated compositions, as well as differences in the predicted CO_2 contents of up to one order of magnitude between the SiO_2-undersaturated leucititic and nephelin-

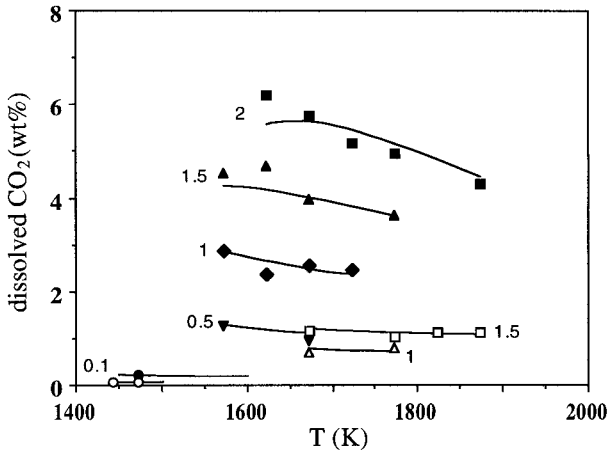

FIGURE 4. Comparison between the experimental data and the model predictions on the CO_2 solubility in silicate liquids of leucititic (filled symbols) and tholeiitic (open symbols) composition as a function of temperature and at different pressures from 0.1 to 2 GPa. The different symbols refer to different pressures (numbers in the figure, in GPa). Experimental data and liquid compositions from Thibault and Holloway (1994) (leucitite) and Pan et al. (1991) (tholeiite).

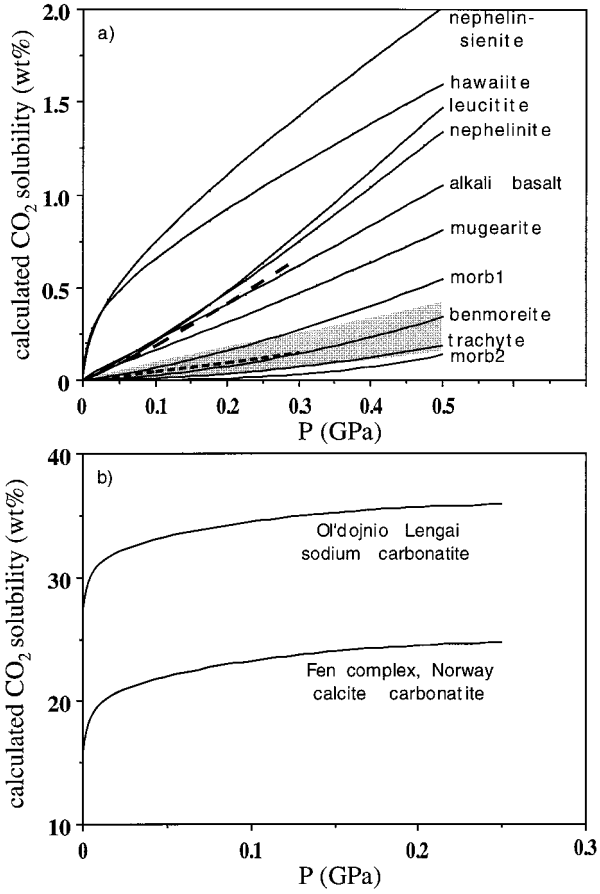

FIGURE 5. Predicted CO_2 solubility as a function of pressure in several liquids of compositions different from those used in the regression of the model parameters. a: silicate liquid compositions, all at T = 1500 K. The stippled area indicates the predicted CO_2 solubility field of liquids from basalt to rhyolite of calcalkaline associations [compositions from Baker (1982), Table 2 nos. 1, 2, 7, and 8]. Other liquid compositions from Barker (1983): nephelinite Table 13–1 no. 2, morb1 and morb2 (tholeiites) Table 11–2 nos. 1 and 2, and D'Amico et al. (1987): alkali basalt, hawaiite, mugearite, benmoreite, and trachite Table 8 nos. 1, 2, 3, 4, 5. Leucititic composition from Thibault and Holloway (1994). The dashed lines are the results of model calculations reported in Dixon (1997) for the CO_2 solubility in a leucititic (upper long-dashed line) and tholeiitic (lower short-dashed line) liquid at T = 1473 K. b: carbonatitic liquid compositions from Barker (1983): sodium carbonatite and calcite carbonatite Table 13–3 nos. 4 and 1, respectively.

itic liquids and the SiO_2-saturated or oversaturated liquids of the calcalkaline suite (stippled area in Fig. 5a) (Holloway and Blank 1994). Along the hawaiite-mugearite-benmoreite-trachyte evolutionary trend, the predicted CO_2 solubility decreases by about 1 order of magnitude (Fig. 5a), whereas within the SiO_2-saturated calcalkaline liquids and at constant temperature, the predicted CO_2 solubility is larger for rhyolitic than for basaltic liquids. The two dashed lines represent the CO_2 solubility at 1473 K for a leucititic (upper long-dashed line) and a tholeiitic liquid (lower short-dashed line), as calculated in Dixon (1997). The agreement with the present model predictions is fairly good, with the curves for the leucititic liquid showing ≤7% deviation and that for the tholeiitic liquid lying between the two calculated curves labeled "morb1" and "morb2."

In Figure 5b, the predicted CO_2 solubility is shown as a function of pressure at T = 800 K for two different liquids of carbonatitic composition. The model correctly predicts very large CO_2 solubilities, consistent with the measured CO_2 contents between 11 and 36 wt% in carbonatitic lavas at atmospheric pressure (Barker 1983).

Water + carbon dioxide

The expressions for the activity coefficients of dissolved H_2O and CO_2 (Eqs. 16 and 17) contain an H_2O-CO_2 interaction term that must be determined in the two-component fluid phase conditions. For this purpose, various expressions corresponding to different possible forms of P-T dependence have been hypothesized in the present work, and the corresponding coefficients have been extracted by least-squares regression of the experimental data. The model predictions produced by using any of the employed expressions for $w_{H_2O\text{-}CO_2}$ differ by <0.1% from those obtained by putting $w_{H_2O\text{-}CO_2} = 0$. As a result, the first term in the right-hand side of Equations 16 and 17 has been neglected.

Several sets of experimental data in the literature refer to the combined $H_2O + CO_2$ solubilities in silicate liquids (e.g., Morey and Fleischer 1940; Kadik et al. 1972; Eggler 1973; Mysen et al. 1975; Mysen 1976; Eggler and Rosenhauer 1978; Eggler and Kadik 1979; Blank et al. 1993; Dixon et al. 1995). Unfortunately, very few of them are useful either for the calibration of the model parameters or for a comparison with the model predictions. Indeed, many of the above-referenced papers do not report the composition of the gas phase at equilibrium or the total amount of each volatile employed in the experiments, which prevents the use of the present model.

A notable exception is the study of Blank et al. (1993) and, to a lesser extent, Dixon et al. (1995), which refer to a rhyolitic composition at T = 1123 K and P = 75 MPa, and tholeiitic composition at T = 1473 K and P in the range 30–100 MPa, respectively. In both cases, the total amounts of H_2O and CO_2 employed in the experiments are known and, with the exception of some of the experiments from Dixon et al. (1995), the relative abundance of H_2O and CO_2 in the fluid phase at equilibrium with the silicate melt was measured. In those cases where the fluid phase composition was not measured, Dixon et al. (1995) recalculated it on the basis of an assumed Henrian behavior of H_2O dissolved in molecular form and an equation from Silver and Stolper (1989) relating the activity of molecular H_2O in the melt to its fugacity in the coexisting fluid. However, this procedure produces discrepancies of up to a factor of 2 in the mole fraction of volatiles in the fluid phase with respect to the mass-balance calculations. This has been attributed by the authors

to open-system conditions relative to H_2 during some of the experiments. In comparing these experimental results with the present model predictions, it was decided to adopt the fluid phase compositions obtained from the mass-balance calculations for two reasons: (1) because the fluid compositions given by Dixon et al. (1995) are model-dependent rather than measured quantities, they cannot be regarded as ''data'' in a strict sense; and (2) because the recalculated values are based on the measured quantities of H_2O dissolved in molecular form but these were not corrected for the temperature of re-equilibration of the reaction $H_2O_{mol} + O^{2-} \leftrightarrow 2OH^-$. Indeed, recent results based on kinetic studies of this reaction in rhyolitic and albitic liquids (Zhang et al. 1995), in-situ infrared spectroscopy in haplogranitic (Nowak and Behrens 1995), and peraluminous sodium (Shenn and Keppler 1995) melts, as well as comparisons between the measured H_2O speciation at room temperature and the determined glass transition temperature in liquids along the join $NaAlSi_3O_8$-$KalSi_3O_8$ (Romano et al. 1995), have all shown that the equilibrium constant for the reaction between molecular and dissociated H_2O is very sensitive to temperature and that the quenched glasses in many experiments preserve an H_2O speciation that corresponds to a temperature much lower than the experimental temperature. These results imply that most of the conclusions based on the speciation of H_2O as measured in quenched glasses should be reconsidered.

Figure 6 compares the combined $H_2O + CO_2$ solubility determinations from Blank et al. (1993) and Dixon et al. (1995) with the model predictions. The agreement between the calculated and experimental compositions of the fluid phase is excellent for both rhyolitic and tholeiitic composition liquids (Fig. 6c). Agreement is good for the dissolved CO_2 and rhyolitic composition but not very satisfactory for the dissolved CO_2 in a tholeiitic composition liquid (Fig. 6b). In the case of the dissolved H_2O (Fig. 6a), the average discrepancy between the model predictions and the data is 13% for the rhyolitic and 30% for the tholeiitic liquid. The disagreement between the predicted and measured dissolved volatile content for some conditions related to the tholeiitic liquid composition may be the consequence of an uncertainty in the effective amount of total H_2O in the system during the experiments, as discussed above. However, it should be noted that the H_2O solubility model is far more accurate for silicate liquids containing small amounts of Fe and Mg oxides, due to the far larger amount of experimental data available on liquids of haplogranitic rather than of basaltic composition (see Papale 1997). Correspondingly, the $H_2O + CO_2$ solubility model predictions are also expected to be more accurate for chemically evolved liquids.

Figure 7 compares the model predictions and the results of the calculations from Gerlach (1986) on the combined $H_2O + CO_2 + S$ solubility in a Kilauean tholeiite as a function of pressure at $T = 1420$ K. As can be seen from the figure, the present model agrees well with the results of those calculations. Both the present model and

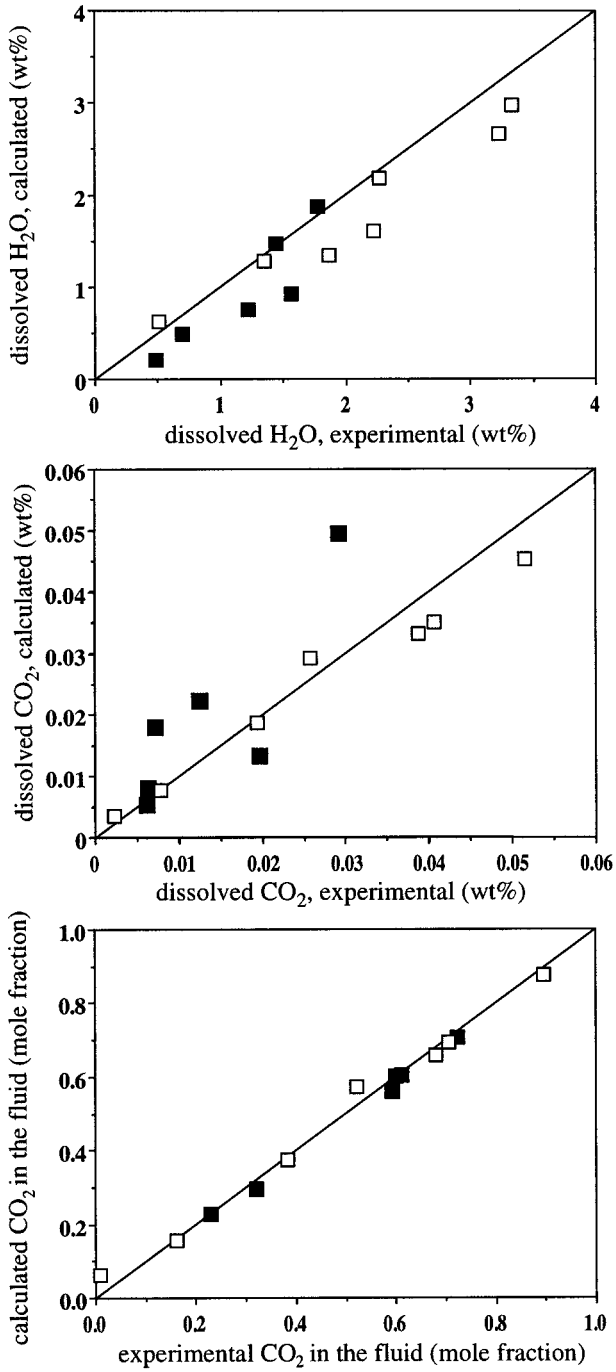

FIGURE 6. Comparison between the experimental and predicted $H_2O + CO_2$ saturation conditions for liquids of rhyolitic (open squares) and tholeiitic (filled squares) compositions at $T = 1123$ and 1473 K, respectively. Experimental data and liquid compositions from Blank et al. (1993) (rhyolite) and Dixon et al. (1995) (tholeiite).

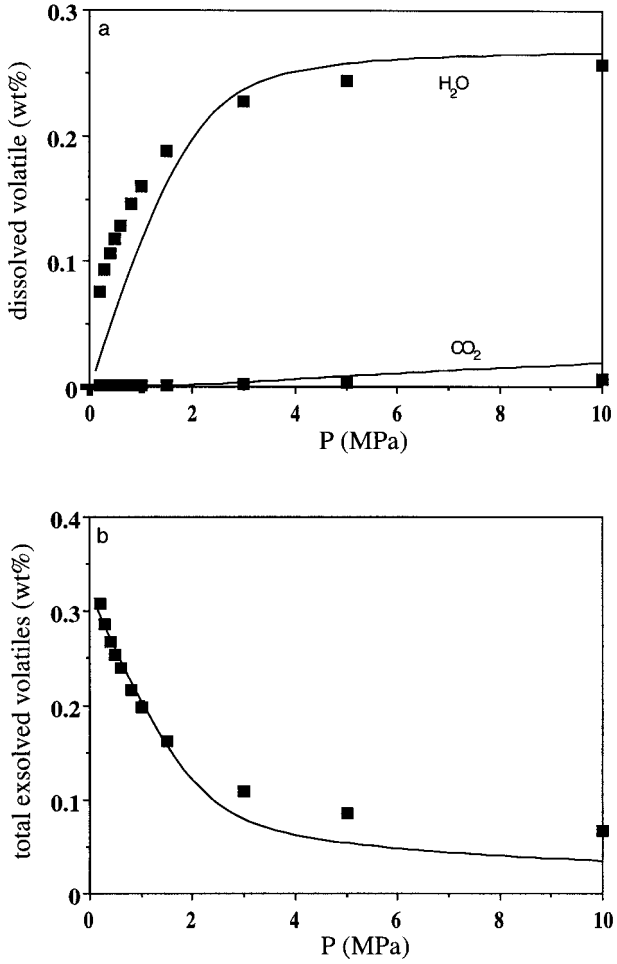

FIGURE 7. Comparison between the predictions of the present model (lines) and those from the model of Gerlach (1986) (symbols) for a Kilauean tholeiitic liquid at T = 1420 K and P from 10 MPa to atmospheric. (**a**) Predicted contents of H_2O + CO_2 at saturation. (**b**) Total exsolved volatiles (wt% with respect to the total magma + initial volatiles). Liquid composition from Harris and Anderson (1983). Total amount of H_2O and CO_2 initially in the system: H_2O = 0.30 wt%, CO_2 = 0.65 wt% (Gerlach 1986).

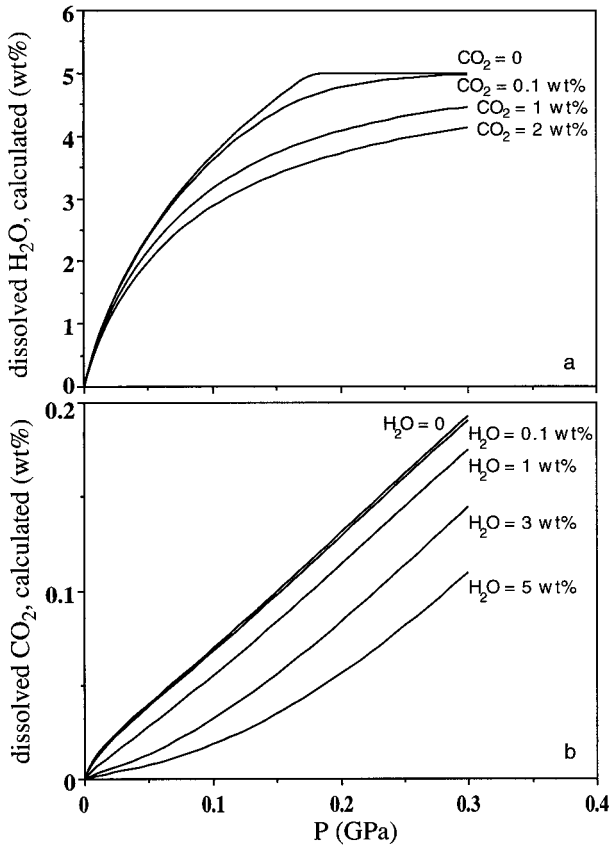

FIGURE 8. Predicted H_2O + CO_2 saturation conditions in a rhyolitic liquid at T = 1123 K as a function of pressure for different ratios of H_2O and CO_2 in the system. (**a**) H_2O content at saturation (assumed total H_2O content = 5 wt%) for total CO_2 contents from 0 to 2 wt%. (**b**) CO_2 content at saturation (assumed total CO_2 content = 2 wt%) for total H_2O contents from 0 to 5 wt%. Liquid composition from Blank et al. (1993).

the simpler model of Gerlach (1986) suggest that most of the available H_2O is retained in the liquid magma up to a very shallow depth (Fig. 7a), and that a significant increase in the amount of the released gas only occurs when the magma approaches the surface (Fig. 7b).

Figure 8 shows the predicted H_2O and CO_2 contents in a rhyolitic liquid at T = 1123 K, P from 0.3 GPa to atmospheric, and different amounts of total H_2O and CO_2 in the system. Note that the progressive addition of one volatile to the system results in a decrease in the dissolved amount of the other one. For example, for a total H_2O content of 5 wt%, the addition of as little as 0.1 wt% of CO_2 has the effect of shifting the saturation pressure from about 0.18 to 0.28 GPa (Fig. 8a). Larger quantities of CO_2 bring about larger increases in the saturation pressure. The addition of 0.1 wt% H_2O has a very small effect on the amount of dissolved CO_2, whereas larger quantities significantly reduce it (Fig. 8b).

The H_2O + CO_2 saturation model can be used in both closed- and open-system conditions. In the first case (closed system), it is assumed that the total amount of each volatile in the system remains constant as the P-T-composition conditions are changed. The curves in Figures 7 and 8 were calculated by assuming closed-system conditions as well as those labeled ''closed'' in Figure 9. The figure refers to liquids of rhyolitic and tholeiitic composition at T = 1123 and 1473 K, respectively, P from 0.2 GPa to atmospheric, and total initial amounts of H_2O and CO_2 of 5 and 0.2 wt% (rhyolite) and 2 and 0.2 wt% (tholeiite). Under open-system conditions (curves labeled as ''open'' in Fig. 9), it is assumed that thermodynamic equilibrium is maintained at each point in P-T space, but during each P-T step, the fluid phase is free to escape from the system so that the total volatile content is reduced progressively. In Figure 9, the curves correspond-

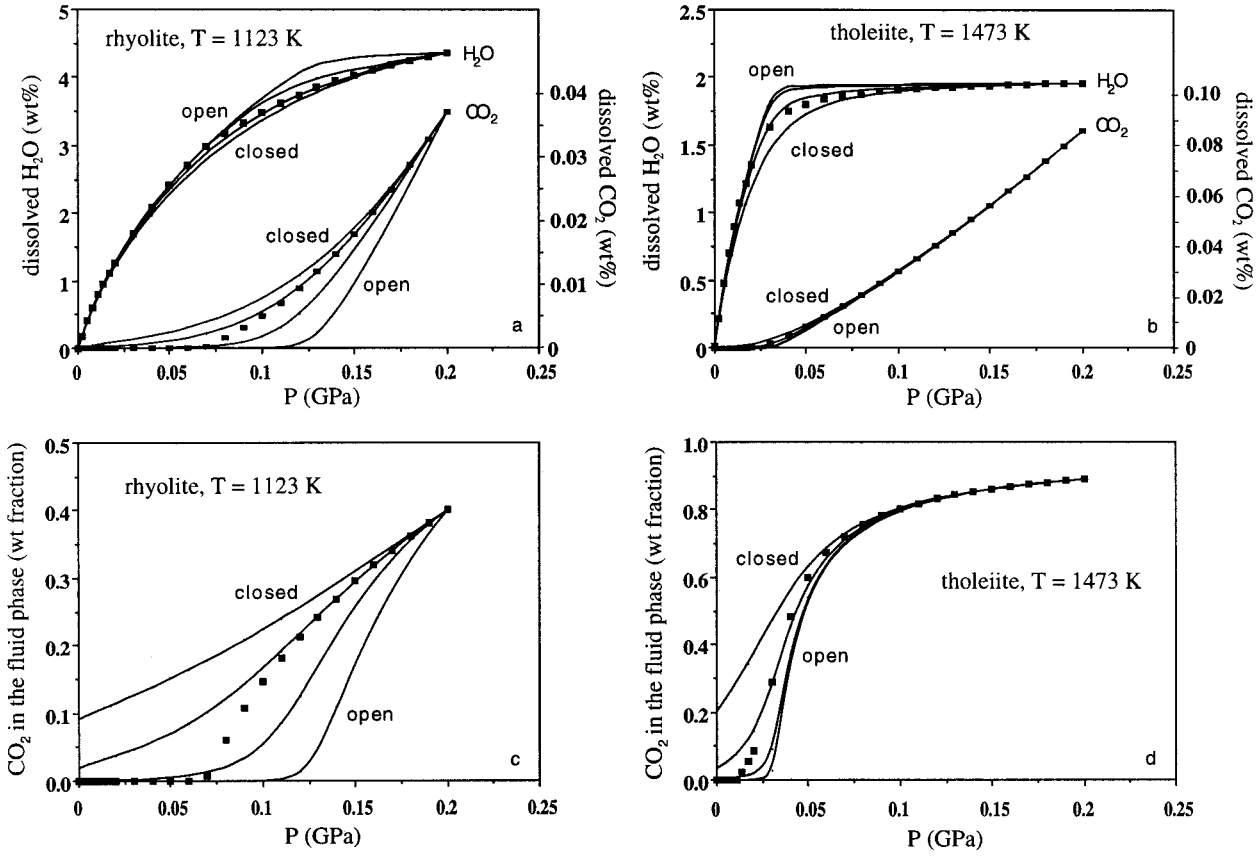

FIGURE 9. Predicted H_2O and CO_2 saturation contents of the liquid and composition of the gas phase in closed- and open-system conditions for two different liquids of rhyolitic and tholeiitic composition at $T = 1123$ and 1173 K, respectively, and P from 0.2 GPa to atmospheric. In each diagram the curves between those labeled as ''closed'' and ''open'' are calculated by assuming a loss of 10 (near the closed system curve) and 30 wt% of the fluid phase, respectively, at each calculation step. The symbols represent the calculations made by assuming that the conditions progressively shift toward those pertaining to open conditions as the pressure is decreased. Liquid compositions from Blank et al. (1993) (rhyolite) and Dixon et al. (1995) (tholeiite). See text for explanation.

ing to a loss of 10 and 30 wt% of the fluid phase at each pressure step are also shown. The closed-system assumption may be appropriate when considering the rapid ascent of a viscous magma during explosive eruptions or the evolution of magma in a magma chamber with sealed walls, whereas the open-system assumption may represent a better approximation for the slow ascent of low-viscosity basaltic magma or the degassing of a magma body below the Earth's surface. It is worth noting that the basic assumption of equilibrium must be satisfied to apply the present model to real situations. As apparent from Figure 9, the predicted saturation curves are significantly different for open- or closed-system conditions. The predicted amount of H_2O in the liquid is enhanced and that of CO_2 is reduced under open-compared with closed-system conditions (Figs. 9a and 9b). This produces important differences in the composition of the coexisting fluid phase. Indeed, in both closed- and open-system conditions, the fluid is predicted to become progressively enriched in H_2O as the pressure decreases. However, this H_2O enrichment is more prominent under open-system conditions where, at a pressure that depends on the specific conditions and that varies from ~50–120 MPa in the examples of Figure 9, CO_2 may be completely exsolved (Figs. 9a and 9b) and the fluid phase made up of pure H_2O (Figs. 9c and 9d). A loss of only 10 wt% of the fluid phase at each P step is sufficient to produce a significant change in its composition, and a loss of 30 wt% produces conditions that resemble those of the open system. Also shown in Figure 9 (filled squares) are the results of calculations made by assuming that the mass of fluids lost from the system increases progressively as the pressure decreases. This situation is likely to be a better approximation of real conditions during the slow ascent of magma because the permeability and fracturization of country rocks normally increase as the depth is reduced allowing a progressively larger mass of fluid to escape from the magma. In this case, the calculated curves diverge progressively from those pertaining to the closed toward those pertaining to the open system, until the fully open

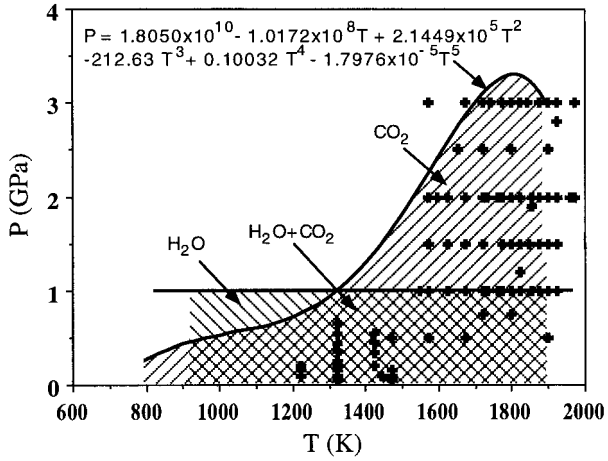

FIGURE 10. Pressure-temperature fields covered by the H_2O, CO_2, and H_2O + CO_2 saturation models. The full line is a fifth-order polynomial approximation of the pressure limit as a function of temperature above which the CO_2 solubility model produces a steep decrease of the predicted CO_2 solubility. The crosses represent the *P-T* conditions corresponding to the experimental CO_2 solubility determinations used to constrain the CO_2 model parameters (references in the caption of Fig. 1).

system curve is reached (depending on the assumed rate of increase of fluid loss).

DISCUSSION

The poor internal consistency of the CO_2 solubility database used in the regression procedure to extract the CO_2 model parameters represents a main difficulty for the modeling of the CO_2 solubility in silicate liquids. The large differences in the predictions obtained by using the model parameters from Appendix Table 1 and those from Papale (1997) (Fig. 2) reflect the high sensitivity of the model to the experimental constraints. The data from recent CO_2 solubility determinations (group 1) appear to be internally consistent (Blank and Brooker 1994; Holloway and Blank 1994), and are reproduced by the model with reasonable accuracy. However, the number of such data (94) compared with the number of model parameters extracted by regression (31, see Appendix 1) has required the inclusion in the database of the less-accurate group 2 data. This situation contrasts markedly with the large number (492) of internally consistent data used for the extraction of the H_2O model parameters (Papale 1997), and produces a significantly greater accuracy of the H_2O-solubility compared with the CO_2-solubility predictions.

A limit to the use of the CO_2-solubility model originates from the fact that when the pressure is increased over a critical value that depends on temperature (and at a second order on liquid composition), the model predicts an unreasonably steep decrease of the CO_2 solubility. This critical pressure is shown as a function of temperature in Figure 10. Note that very few experimental data utilized in the database refer to conditions above this critical pressure, possibly because at such *P-T* conditions the tendency of liquids to partially crystallize becomes too large to be controlled during the experiments. The critical line in Figure 10 thus represents an upper limit for the application of the CO_2 solubility model. Also shown in Figure 10 is the upper limit for the application of the H_2O solubility model (from Papale 1997). The intersection of the two fields gives the *P-T* region where the H_2O + CO_2 model can be applied. This includes most of the *P-T* conditions relevant to the volcanic environment.

Based on the low-pressure experimental determinations of the saturation surface of a two-component H_2O + CO_2 fluid in silicate liquids, it has been suggested (Blank et al. 1993; Dixon et al. 1995; Dixon and Stolper 1995; Holloway and Blank 1994) that the amount of dissolved H_2O and CO_2 at low pressure can be obtained from the solubilities of pure H_2O and pure CO_2 at the same conditions and at a reduced fugacity corresponding to that in the two-component H_2O + CO_2 fluid. In this view, the effect of the two-component nature of the fluid phase is just that of diluting each volatile in the fluid, whereas no significant effect is produced by the simultaneous presence of the two volatiles in the liquid. This behavior can be expressed by an isobaric-isothermal form of the Henry's law for the dissolved H_2O and CO_2:

$$x_i = H_i f_i^G \quad (P, T, x' = \text{constant}) \tag{18}$$

where H is the Henry's constant, which depends on pressure, temperature, and composition, x' indicates the silicate liquid composition as normalized without volatiles, and i = H_2O or CO_2. Equation 18 implies that x_{H_2O} (or x_{CO_2}) is neglected in the expression of the activity coefficient of dissolved CO_2 (or H_2O), Equation 17 (or Eq. 16). At a pressure of 1 GPa, the H_2O + CO_2 saturation data of Jacobsson (1997) show an essentially constant amount of CO_2 in an icelanditic melt at 1673 K despite a three-fold variation in the CO_2 fugacity in the fluid phase at equilibrium. This implies that Equation 18 does not hold at that condition, i.e., the liquid-fluid equilibrium cannot be described by Henry's law at 1 GPa. At higher pressures between 2 and 4 GPa, the results of Mysen and co-workers (Mysen 1976; Mysen et al. 1976), although less accurate as discussed above, show that the amount of dissolved CO_2 at isobaric-isothermal conditions may increase significantly when H_2O is added to a pure CO_2 fluid, which is contrary to the predictions of Henry's law as defined in Equation 18. Thus, the picture that emerges from the experimental data on H_2O + CO_2 dissolution in silicate liquids is that with increasing pressure, the equilibrium condition progressively moves from Henrian to strongly non-Henrian. In Figure 11 fugacity-composition relationships are shown based on the present model for rhyolitic and tholeiitic liquids at T = 1123 and 1473 K, respectively, and P = 0.01, 0.1, 0.3, and 0.5 GPa. In each diagram of the figure, the normalized dissolved volatile content, x_i^*, is plotted against the normalized fugacity in the fluid phase, f_i^*G (i = H_2O or CO_2), where the normalization is made with respect to the one-component

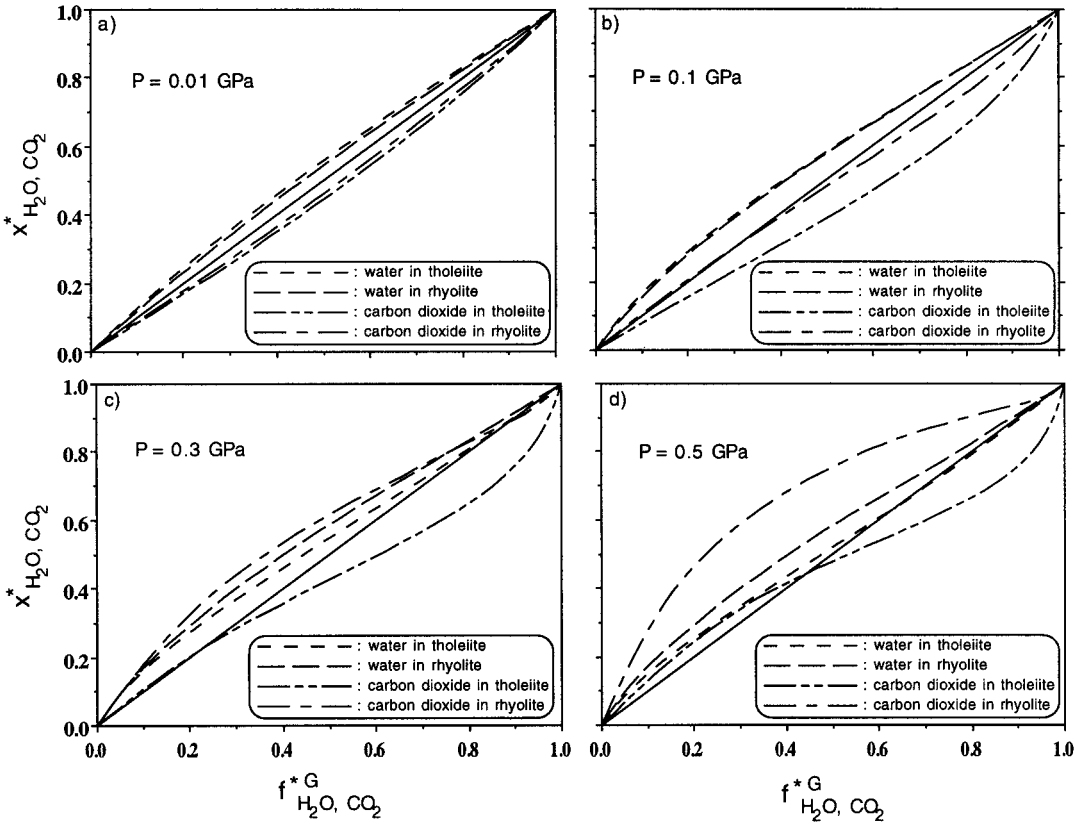

FIGURE 11. Predicted normalized H_2O and CO_2 contents as a function of the normalized fugacity of the corresponding component in the fluid phase at equilibrium for two different liquids of rhyolitic and tholeiitic composition at $T = 1123$ and 1473 K, respectively, and four different pressures from 0.01 to 0.5 GPa. In each diagram the solid line corresponds to Henrian behavior as given by Equation 18. Liquid compositions from Blank et al. (1993) (rhyolite) and Dixon et al. (1995) (tholeiite). See text for the details of the normalization.

fluid phase at the same *P-T*-liquid composition conditions:

$$x_i^* = \frac{x_{i\mathrm{H_2O+CO_2}}}{x_{i\mathrm{pure}\,i}}; \qquad f_i^{*G} = \frac{f^G_{i\mathrm{H_2O+CO_2}}}{f^G_{i\mathrm{pure}\,i}} \tag{19}$$

A Henrian behavior like that of Equation 18 would plot in the diagrams of Figure 11 along the diagonal solid lines. As evident in the figure, the predicted behavior of H_2O and CO_2 is not strictly Henrian at any considered pressure, but at low pressure or for some given range of dissolved H_2O and CO_2, it may effectively approximate a Henrian behavior. This is well shown in Figure 11a, which refers to 0.01 GPa. At 0.1 GPa (Fig. 11b), the behavior is still nearly Henrian for the rhyolitic composition but shows significant negative deviations for CO_2 in a tholeiitic composition. At larger pressure the deviations—either positive or negative—become significant for CO_2 in both rhyolitic and tholeiitic compositions, whereas H_2O continues to show small positive deviations from Henrian behavior (Figs. 11c and 11d). The results of the modeling agree with those from Blank et al. (1993) on rhyolitic liquids at 75 MPa and partly with those from Dixon et al. (1995) on tholeiitic liquids at 30–100 MPa pressure. The deviations from Henrian behavior in Figure 11 do not result from an H_2O-CO_2 interaction in the liquid phase because, as explained above, this interaction is neglected in the present model. Rather, the deviations arise from the fact that each dissolved volatile effectively modifies the liquid composition by modifying the mole fractions of all the other components. From a molecular point of view, this means that the average number of ions (or molecules) of each given species surrounding, for example, the molecules of the dissolved CO_2 (either molecular CO_2 or carbonate ions) is progressively reduced when more H_2O is dissolved in the liquid. This is expressed in Equations 16 and 17 by the dependence of the activity coefficient of each volatile on the mole fraction of the other dissolved volatile. Thus, when two volatile components are present, a dilution effect similar to that occurring in the fluid phase also occurs in the liquid phase, and its importance increases with increasing pressure, i.e., with increasing amount of dissolved volatiles.

Many of the above results pertaining to rhyolitic and tholeiitic liquids, which are used extensively in the present paper to illustrate the model predictions are embodied in the two diagrams of Figure 12. In these diagrams,

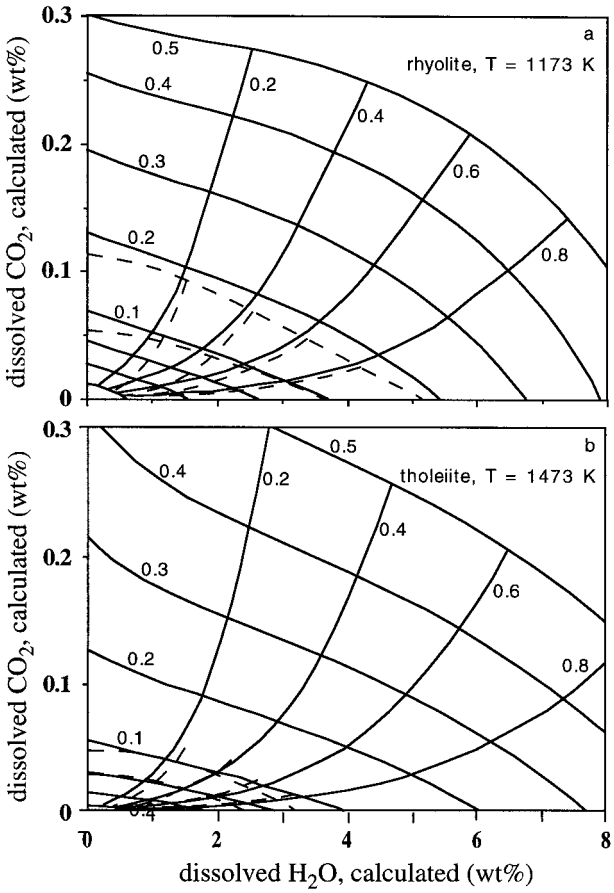

FIGURE 12. Predicted dissolved amount of CO_2 and composition of the fluid phase at equilibrium, as a function of the dissolved amount of H_2O in two liquids of rhyolitic (**a**) and tholeiitic (**b**) composition at T = 1173 and 1473 K, respectively. In each diagram the numbers on the descending solid lines represent the pressure (GPa). The first three unlabeled lines at the bottom of each diagram refer to P = 0.01, 0.03, and 0.06 GPa, respectively. The ascending solid lines join all the points in the diagram in equilibrium with a fluid of the same composition, given in values of y_{H_2O}. The dashed lines in the lower part of each diagram represent the calculations from Holloway and Blank (1994) and Dixon and Stolper (1995) made by assuming a Henrian behavior of H_2O and CO_2 in the liquid as defined in Equation 18, and correspond to P = 0.1 and 0.2 GPa (rhyolite) and P = 0.06 and 0.1 GPa (tholeiite); the composition of the fluid phase pertaining to the ascending dashed lines is the same as for the present calculations. Liquid composition from Blank et al. (1993) (rhyolite) and Pawley et al. (1992) (tholeiite).

the descending full lines represent the predicted equilibrium contents of H_2O and CO_2 in the liquid at the indicated temperature and several different pressures from 10 MPa to 0.5 GPa. The ascending full lines join all the equilibrium distributions of H_2O and CO_2 in the liquid corresponding to the same values of y_{H_2O} in the coexisting fluid phase. The low-pressure curves (up to 0.2 GPa) in Figure 12 substantially agree with the corresponding curves from Dixon and Stolper (1995), Dixon (1997), and

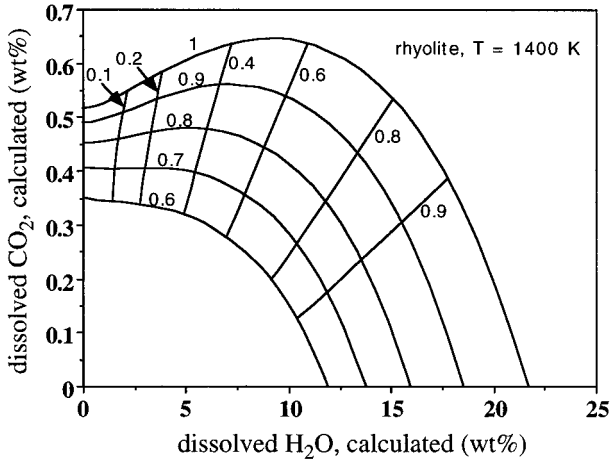

FIGURE 13. Predicted amount of dissolved CO_2 at high pressure (0.6–1 GPa) and composition of the fluid phase at equilibrium, as a function of the dissolved amount of H_2O for the same rhyolitic composition as in Figure 12 and T = 1400 K. Explanation as in the caption of Figure 12.

Holloway and Blank (1994) (dashed lines in the figure), which were calculated by assuming a Henrian behavior of H_2O and CO_2 in the liquid as defined in Equation 18. In contrast to these earlier models, the present H_2O + CO_2 saturation model allows predictions to be made up to several tenths of GPa. Figure 13 shows the case of a rhyolitic liquid at pressure from 0.6 to 1 GPa. As evident in this figure, the predicted effect of the addition of water to a pure CO_2 fluid at high pressure is not simply that of reducing the dissolved amount of CO_2. At a pressure from 0.6 to 0.8 GPa, this effect progressively changes from a decrease to an increase in the amount of dissolved CO_2. At 0.7 GPa, the calculated dissolved CO_2 is about constant in a range of fluid phase compositions from y_{CO_2} = 1.0 to ~0.6, which corresponds to a two-fold variation in the CO_2 fugacity in the fluid phase. At a pressure of 0.9–1 GPa, the addition of a small amount of H_2O to pure CO_2 produces a 13–25% increase in the amount of dissolved CO_2 up to y_{H_2O} ~0.5.

The present model does not pretend to be accurate at such high pressures, as it was shown in Papale (1997) that the accuracy of the H_2O solubility predictions progressively worsen as the pressure approaches 1 GPa. This is clearly shown by the fact that, when applied to an icelanditic melt at 1 GPa and 1673 K, the present model correctly predicts the CO_2 solubility at about 1.2 wt% and a strong non-Henrian behavior of the H_2O + CO_2 fluid-liquid equilibrium. However, the addition of H_2O up to y_{H_2O} ~0.4 produces a 30% decrease in the amount of dissolved CO_2, whereas the experimental results from Jacobsson (1997) produced a constant amount of dissolved CO_2. This discrepancy is also related to the fact that, as discussed in Papale (1997), the accuracy of the predictions about the dissolved H_2O decreases when the liquid composition becomes more mafic, due to a lack of pub-

lished H_2O solubility data for mafic liquids. Nonetheless, the present model predicts that as pressure increases from <0.1 GPa to several tenths of GPa, a progressive shift from essentially Henrian to non-Henrian behavior occurs (Fig. 11); the present model also predicts a progressive change from negative to positive slopes of the equilibrium curves in Figures 12 and 13 close to the pure CO_2 side of the diagrams. This predicted behavior corresponds to the observed essentially Henrian low-*P* experimental results of Blank et al. (1993) and Dixon et al. (1995), to the high-*P* non-Henrian results of Jacobsson (1997), and to the very high-*P* strongly non-Henrian results of Mysen (1976) and Mysen et al. (1976). According to Jacobsson (1997), such non-Henrian behavior is produced by the structural and compositional changes that accompany the dissolution of large amounts of H_2O in the silicate liquid at high pressure. The present model confirms this hypothesis, by including the important modifications of the excess Gibbs free energy and thus of the activity-composition relationships of CO_2 due to the dissolution of large amounts of H_2O. This modeling result is obtained thanks to a description of the excess Gibbs free energy of the silicate liquid as a complex function of liquid composition including dissolved volatiles, thus accounting for the dependence of the activity of each volatile on the amount of the other dissolved volatile (Eqs. 16 and 17).

ACKNOWLEDGMENTS

This work was supported by the Gruppo Nazionale per la Vulcanologia of Italy and was performed in the ambience of the Volcanic Simulation Group in Pisa. The author is grateful to Giovanni Macedonio for his continuous support. The paper has benefited of a critical reading from Augusto Neri.

REFERENCES CITED

Baker, P.E. (1982) Evolution and classification of orogenic volcanic rocks. In R.S. Thorpe, Ed., Andesites, p. 11–23. Wiley, New York.

Barker, D.S. (1983) Igneous rocks, 417 p. Prentice-Hall, Englewood Cliffs, New Jersey.

Blank, J.G. and Brooker, R.A. (1994) Experimental studies of carbon dioxide in silicate melts: solubility, speciation, and stable carbon isotope behavior. In Mineralogical Society of America Reviews in Mineralogy, 30, 157–186.

Blank, J.G., Stolper, E.M., and Carroll, M.R. (1993) Solubilities of carbon dioxide and water in rhyolitic melt at 850 °C and 750 bars. Earth and Planetary Science Letters, 119, 27–36.

Brey, G. (1976) CO_2 solubility and solubility mechanisms in silicate melts at high pressure. Contributions to Mineralogy and Petrology, 57, 215–221.

Brey, G. and Green, D.H. (1975) The role of CO_2 in the genesis of olivine melilitite. Contributions to Mineralogy and Petrology, 49, 93–103.

——— (1976) Solubility of CO_2 in olivine melilitite at high pressure and role of CO_2 in the Earth's upper mantle. Contributions to Mineralogy and Petrology, 55, 217–230.

D'Amico, C., Innocenti, F., and Sassi, F.P. (1987) Magmatismo e metamorfismo, 536 p. Unione Tipografico-Editrice Torinese (UTET), Torino (in Italian).

Dixon, J.E. (1997) Degassing of alkalic basalts. American Mineralogist, 82, 368–378.

Dixon, J.E. and Stolper, E.M. (1995) An experimental study of water and carbon dioxide solubilities in mid-ocean ridge basaltic liquids. Part II: applications to degassing. Journal of Petrology, 36, 1633–1646.

Dixon, J.E., Stolper, E.M., and Holloway, J.R. (1995) An experimental study of water and carbon dioxide solubilities in mid-ocean ridge basaltic liquids. Part I: calibration and solubility models. Journal of Petrology, 36, 1607–1631.

Eggler, D.H. (1973) Role of CO_2 in melting processes in the mantle. Carnegie Institution of Washington Yearbook, 72, 457–467.

Eggler, D.H. and Kadik, A.A. (1979) The system $NaAlSi_3O_8$-H_2O-CO_2 to 20 kbar pressure: I. Compositional and thermodynamic relations of liquids and vapors coexisting with albite. American Mineralogist, 64, 1036–1048.

Eggler, D.H. and Mysen, B.O. (1976) The role of CO_2 in the genesis of olivine melilitite: discussion. Contributions to Mineralogy and Petrology, 55, 231–236.

Eggler, D.H. and Rosenhauer, M. (1978) Carbon dioxide in silicate melts. II. Solubilities of CO_2 and H_2O in $CaMgSi_2O_6$ (diopside) liquids and vapors at pressures to 40 kilobars. American Journal of Science, 278, 64–94.

Fogel, R.A. and Rutherford, M.J. (1990) The solubility of carbon dioxide in rhyolitic melts: a quantitative FTIR study. American Mineralogist, 75, 1311–1326.

Gerlach, T.M. (1986) Exsolution of H_2O, CO_2, and S during eruptive episodes at Kilauea volcano, Hawaii. Journal of Geophysical Research, 91, 12,177–12,185.

Ghiorso, M.S., Carmichael, I.S.E., Rivers, M.L., and Sack, R.O. (1983) The Gibbs free energy of mixing of natural silicate liquids; an expanded regular solution approximation for the calculation of magmatic intensive variables. Contributions to Mineralogy and Petrology, 84, 107–145.

Hamilton, D.L., Burnham, C.W., and Osborn, E.F. (1964) The solubility of water and effects of oxygen fugacity and water content on crystallization in mafic magmas. Journal of Petrology, 5, 21–39.

Harris, D.M. and Anderson, A.T. Jr. (1983) Concentrations, sources, and losses of H_2O, CO_2, and S in Kilauea basalt. Geochimica et Cosmochimica Acta, 47, 1139–1150.

Holloway, J.R. and Blank, J.G. (1994) Application of experimental results to C-O-H species in natural melts. In Mineralogical Society of America Reviews in Mineralogy, 30, 187–230.

Holloway, J.R., Mysen, B.O., and Eggler, D.H. (1976) The solubility of CO_2 in liquids on the join CaO-MgO-SiO_2-CO_2. Carnegie Institution of Washington Yearbook, 75, 626–631.

Holtz, F., Behrens, H., Dingwell, D.B., and Johannes, W. (1995) H_2O solubility in haplogranitic melts: compositional, pressure, and temperature dependence. American Mineralogist, 80, 94–108.

Jacobsson, S. (1997) Solubility of water and carbon dioxide in an icelandite at 1400 °C and 10 kilobars. Contributions to Mineralogy and Petrology, 127, 129–135.

Kadik, A.A., Lukanin, O.A., Lebedev, Y.B., and Korovushkina, E.Y. (1972) Solubility of H_2O and CO_2 in granite and basalt melts at high pressures. Geochimiya, 12, 1549–1560.

Kerrick, D.M. and Jacobs, G.K. (1981) A modified Redlich-Kwong equation for H_2O, CO_2, and H_2O-CO_2 mixtures at elevated pressures and temperatures. American Journal of Science, 281, 735–767.

Lange, R.A. (1994) The effect of H_2O, CO_2 and F on the density and viscosity of silicate melts. In Mineralogical Society of America Reviews in Mineralogy, 30, 331–369.

Mattey, D.P., Taylor, W.R., Green, D.H., and Pillinger, C.T. (1990) Carbon isotopic fractionation between CO_2 vapor, silicate and carbonate melts: an experimental study to 30 kbar. Contributions to Mineralogy and Petrology, 104, 492–505.

McMillan, P.F. (1994) Water solubility and speciation models. In Mineralogical Society of America Reviews in Mineralogy, 30, 131–156.

Morey, G.W. and Fleischer, M. (1940) Equilibrium between vapor and liquid phases in the system CO_2-H_2O-K_2O-SiO_2. Bullettin of the Geological Society of America, 51, 1035–1058.

Mysen, B.O. (1976) The role of volatiles in silicate melts: solubility of carbon dioxide and water in feldspar, pyroxene, and feldspathoid melts to 30 kb and 1625 °C. American Journal of Science, 276, 969–996.

Mysen, B.O., and Virgo, D. (1980a) Solubility mechanisms of carbon dioxide in silicate melts: a Raman spectroscopic study. American Mineralogist, 65, 885–899.

——— (1980b) The solubility behavior of CO_2 in melts on the join $NaAlSi_3O_8$-$CaAl_2Si_2O_8$-CO_2 at high pressure and temperature: a Raman spectroscopic study. American Mineralogist, 65, 1166–1175.

Mysen, B.O., Seitz, M.G., and Frantz, J.D. (1974) Measurements of the solubility of carbon dioxide in silicate melts utilizing maps of carbon-14 beta activity. Carnegie Institution of Washington Yearbook, 73, 224–226.

Mysen, B.O., Arculus, R.J., and Eggler, D.H. (1975) Solubility of carbon dioxide in natural nephelinite, tholeiite and andesite melts to 30 kbar pressure. Contributions to Mineralogy and Petrology, 53, 227–239.

Mysen, B.O., Eggler, D.H., Seitz, M.G., and Holloway, J.R. (1976) Carbon dioxide solubilities in silicate melts and crystals. Part I. Solubility measurements. American Journal of Science, 276, 455–479.

Nowak, M. and Behrens, H. (1995) The speciation of water in haplogranitic glasses and melts determined by in situ near-infrared spectroscopy. Geochimica et Cosmochimica Acta, 59, 3445–3450.

Paillat, O., Elphick, S.C., and Brown, W.L. (1992) The solubility of water in $NaAlSi_3O_8$ melts: a re-examination of Ab-H_2O phase relationships and critical behaviour at high pressures. Contributions to Mineralogy and Petrology, 112, 490–500.

Pan, V., Holloway, J.R., and Hervig, R.L. (1991) The pressure and temperature dependence of carbon dioxide solubility in tholeiitic basalt melts. Geochimica et Cosmochimica Acta, 55, 1587–1595.

Papale, P. (1997) Thermodynamic modeling of the solubility of H_2O and CO_2 in silicate liquids. Contributions to Mineralogy and Petrology, 126, 237–251.

Papale, P., Neri, A., and Macedonio, G. (1998) The role of magma composition and water content in explosive eruptions. 1. Conduit ascent dynamics. Journal of Volcanology and Geothermal Research, in press.

Pawley, A.R., Holloway, J.R., and McMillan, P.F. (1992) The effect of oxygen fugacity on the solubility of carbon-oxygen fluids in basaltic melt. Earth and Planetary Science Letters, 110, 213–225.

Press, W.M., Teukolski, S.A., Vetterling, W.T., and Flannery, B.P. (1992) Numerical recipes in FORTRAN—The art of scientific computing, second edition, 963 p. Cambridge University Press Cambridge, U.K.

Rai, C.S., Sharma, S.K., Meunow, D.W., Matson, D.W., and Byers, C.D. (1983) Temperature dependence of CO_2 solubility in high pressure quenched glass of diopside composition. Geochimica et Cosmochimica Acta, 47, 953–958.

Romano, C., Dingwell, D.B., and Behrens, H. (1995) The temperature dependence of the speciation of water in $NaAlSi_3O_8$-$KalSi_3O_8$ melts: an application of fictive temperatures derived from synthetic fluid inclusions. Contributions to Mineralogy and Petrology, 122, 1–10.

Shenn, A. and Keppler, H. (1995) Infrared spectroscopy of hydrous silicate melts to 1000 °C and 10 kbar: direct observation of H_2O speciation in a diamond-anvil cell. American Mineralogist, 80, 1335–1338.

Silver, L. and Stolper, E.M. (1989) Water in albitic glasses. Journal of Petrology, 30, 667–709.

Stolper, E.M., Fine, G.J., Johnson, T., and Newman, S. (1987) The solubility of carbon dioxide in albitic melt. American Mineralogist, 72, 1071–1085.

Tait, S., Jaupart, C., and Vergnoille, S. (1989) Pressure, gas content and eruption periodicity of a shallow, crystallyzing magma chamber. Earth and Planetary Science Letters, 92, 107–123.

Thibault, Y. and Holloway, J.R. (1994) Solubility of CO_2 in a Ca-rich leucitite: effects of pressure, temperature and oxygen fugacity. Contributions to Mineralogy and Petrology, 116, 216–224.

Tuttle, O.F. and Bowen, N.L. (1958) Origin of granite in the light of experimental studies in the system $NaAlSi_3O_8$-$KAlSi_3O_8$-SiO_2-H_2O. Geological Society of America Memories, 74, 1–154.

Zhang, Y., Stolper, E.M., and Ihinger, P.D. (1995) Kinetics of the reaction $H_2O + O = 2OH$ in rhyolitic and albitic glasses: preliminary results. American Mineralogist, 80, 593–612.

APPENDIX 1: LEAST-SQUARES REGRESSION PROCEDURE

As explained in the text, the CO_2-related model parameters are calibrated by least-squares fitting of many experimental determinations. The basic assumption underlying least-squares regression is that each data point has a measurement error that is distributed as a normal (Gaussian) distribution around the ''true'' value. On this basis, the estimation of maximum likelihood of a given set of model parameters corresponds to the minimization of chi-square χ^2 given by:

$$\chi^2 = \sum_{i=1}^{N} \left[\frac{b_i - b(x_i, p_1, \cdots, p_M)}{\sigma_i} \right]^2 \qquad (A.1)$$

where b_i is the measured dependent variable that is a function of the independent variable x_i and of M model parameters $p_1, \cdots, p_M$, σ_i is the standard deviation of the i^{th} data point, and the summation is extended to N data points. However, the minimization of χ^2 does not guarantee that the adopted model is really a good one. Indeed, it is the chi-square probability function, $P(\chi^2, \nu)$, where $\nu = N\text{-}M$ is the number of degrees of freedom (i.e., the number of observations in excess of those necessary to determine the model parameters), which gives a quantitative measurement of the goodness-of-fit. $P(\chi^2, \nu)$ corresponds to the probability of observing a value of chi-square larger than the calculated χ^2 for a random sample of N observations with ν degrees of freedom, and is given by (Bevington 1969):

$$P(\chi^2, \nu) = \frac{1}{2^{\nu/2}\Gamma\left(\frac{\nu}{2}\right)} \int_{\chi^2}^{\infty} (x^2)^{(\nu-2)/2} e^{-(x^2/2)}\, d(x^2) \qquad (A.2)$$

where $\Gamma(\nu/2)$ is the gamma function evaluated at $\nu/2$. The chi-square probability function has the limiting values $P(0, \nu) = 1$, $P(\infty, \nu) = 0$. Values of $P(\chi^2, \nu)$ that approximate both limiting values are in general symptoms of some troubles with the model or the data, and are a typical consequence of a bad estimate of the measurement error associated with the data and expressed by their standard deviation. This point is crucial in the present case. Indeed, least-squares regression as a means of extracting model parameters is more efficient the more its basic assumption is satisfied, i.e., the more the measurement errors are normally (or randomly) distributed. In such conditions the standard deviation, σ_i, associated with each data point is given by:

$$\sigma_i = \left[\sum_j \left(\frac{\partial b_i}{\partial q_j} \Delta q_j \right)^2 \right]^{1/2} \qquad (A.3)$$

where q_j is the j^{th} system variable (e.g., pressure, temperature, and so on) with experimental uncertainty Δq_j. In the present case, the large internal inconsistency of CO_2 solubility data (see for example Fig. 2) is evidence of the occurrence of systematic rather than random measurement errors. This results in a departure from the ideal condition for application of least-squares regression techniques, and yields model predictions that show both small errors for many data points and large errors for some of them. This last case leads to the notion of outliers, i.e., data points that lie out of the fit of the main body of data. In the attempt to include these points in the fit, the least-squares regression may result in a wrong estimate of the model parameters. This occurs even if the outlying points are a small fraction of the data points in the database.

APPENDIX TABLE 1. Parameters of the carbon dioxide solubility model

Parameter	Calibr. value
$\omega^{(0)}_{CO_2-SiO_2}$	−296 439.65
$\omega^{(0)}_{CO_2-TiO_2}$	−7825 041.4
$\omega^{(0)}_{CO_2-Al_2O_3}$	1292 698.7
$\omega^{(0)}_{CO_2-Fe_2O_3}$	755 789.44
$\omega^{(0)}_{CO_2-FeO}$	−295 239.84
$\omega^{(0)}_{CO_2-MnO}$	8418 180.9
$\omega^{(0)}_{CO_2-MgO}$	744 380.60
$\omega^{(0)}_{CO_2-CaO}$	−684 410.66
$\omega^{(0)}_{CO_2-Na_2O}$	−905 549.57
$\omega^{(0)}_{CO_2-K_2O}$	812 898.73
$\omega^{(1)}_{CO_2-SiO_2}$	30543.036
$\omega^{(1)}_{CO_2-TiO_2}$	768 639.85
$\omega^{(1)}_{CO_2-Al_2O_3}$	−158 145.12
$\omega^{(1)}_{CO_2-Fe_2O_3}$	−86808.309
$\omega^{(1)}_{CO_2-FeO}$	39992.274
$\omega^{(1)}_{CO_2-MnO}$	−1074 901.1
$\omega^{(1)}_{CO_2-MgO}$	−84669.749
$\omega^{(1)}_{CO_2-CaO}$	46429.353
$\omega^{(1)}_{CO_2-Na_2O}$	71860.047
$\omega^{(1)}_{CO_2-K_2O}$	−115 526.30
a_1	1.3089×10^{-4}
a_2	-3.1556×10^{-7}
a_3	2.4984×10^{-10}
a_4	-5.9574×10^{-14}
a_5	2.5991×10^{-13}
a_6	-2.8705×10^{-16}
a_7	8.2935×10^{-20}
a_8	-4.4169×10^{-24}
a_9	9.8291×10^{-28}
a_{10}	1.1255×10^{-33}
$\ln f^0_{CO_2}(P^0_{CO_2}, T^0_{CO_2})$	24.161 808
$T^{0\,*}_{CO_2}$	1400
$P^{0\,*}_{CO_2}$	0

Note: Units are I.S.
* Not calibrated by regression.

The numerical procedures that are designed appositely to prevent the inconveniences due to the presence of outlying points in the database constitute the object of the robust estimate techniques (Press et al. 1986). These techniques are based on the identification of such outliers and their processing in a different way. In the present paper, a numerical procedure was designed that automatically identifies and excludes the outliers from the database. This procedure consists of the following steps.

(1) Estimation of the standard deviation, σ_i, for all data points by using Equation A3 with q equal to P and T. The data for which the experimental uncertainties in the nominal P and T are not indicated have been included by assigning uncertainties similar to those reported for other solubility experiments made with similar apparatus in the same P-T range.

(2) Identification of the less-accurate data, based on the abundant literature indicating that the pre-1980 CO_2 solubility data are affected by systematic errors. An experimental uncertainty ten times larger than the nominal uncertainty was assigned to these data.

(3) Extract the model parameters by minimization of the χ^2 value given by Equation A1.

(4) Find the outliers, and repeat step 3 by excluding them from the database. In this paper a given data point is treated as an outlier if its squared weighted residual—i.e., its contribution to the χ^2 value—is larger than 3. In the case that no outliers are found, move to the following step.

(5) Calculate the chi-square probability function $P(\chi^2, \nu)$ from Equation A2. A rule of thumb is that a typical value of $P(\chi^2, \nu)$ for a ''moderately good'' fit is $0.05 < P(\chi^2, \nu) < 0.95$, corresponding to $\chi^2 \approx \nu$ (Press et al. 1986). If the value of the chi-square probability function falls inside these limiting values, then the least-squares regression procedure is terminated, otherwise all the standard deviations are multiplied by a convenient factor and the procedure is repeated from step 3.

The result of the above procedure is reported in Appendix Table 1. Obviously, this procedure rules out the possibility of an independent measurement of the ''goodness-of-fit,'' since the original standard deviations of the experimental data are altered until the normalized chi-square χ^2/ν is about 1. On the other hand, in the present case such measurement is not meaningful even if the original standard deviations are retained, since as explained above (and illustrated in Fig. 2) in many cases such deviations are just related to the reproducibility of a given solubility measurement with that experimental apparatus and technique, while other techniques may produce largely different results.

The inclusion of data points with large assigned errors also produces large standard deviations of the calibrated model parameters, which in many cases are on the same order of magnitude as the model parameter itself. On the other hand, if only the accurate post-1980 CO_2 solubility data are processed, the calibrated model parameters are associated with much smaller standard deviations (from 1 to 3 orders of magnitude less than the calibrated value) but the model predictions become unstable to small compositional changes, i.e., the model reproduces with increased degree of confidence the database but it loses the capability to extend its predictions to different compositions. *The present calibration thus represents a sort of compromise between accuracy and generality.* The validity of the model in a wide spectrum of conditions can be assessed by comparing the model predictions with the experimental data, or by evaluating the capability of the model to predict features of the H_2O + CO_2 saturation surface that are being reconstructed from the experimental data, as the progressive deviation from Henrian behavior as defined in Equation 18 when the pressure is increased from less than one to several tenths of GPa.

APPENDIX 2: SYNTHETIC DESCRIPTION OF THE EMPLOYED DATABASE

The database employed in the regression of the CO_2-related model parameters corresponds to that described in Papale (1997) with the addition of 26 constraints produced by 13 H_2O + CO_2 fluid saturation determinations from Blank et al. (1993) on a rhyolitic liquid and from Dixon et al. (1995) on a tholeiitic liquid. As reported in the text and in Appendix 1, the total number of experimental constraints used in the calibration is 289, 120 of

APPENDIX TABLE 2. Synthetic description of the employed database

Oxide	Abundance (wt%)	*P* (MPa)	*T* (K)
SiO_2	37.0–77.7	31–4000	1173–1885
	(37.0–77.7)	(31–4000)	(1173–2063)
TiO_2	0.07–2.96	31–1513	1173–1813
	(0.07–2.96)	(31–4000)	(1173–1973)
Al_2O_3	11.1–23.9	31–4000	1173–1885
	(4.71–36.7)	(31–4000)	(1173–2063)
Fe_2O_3	0.19–2.84	31–3000	1173–1623
	(0.19–4.60)	(31–3000)	(1173–1923)
FeO	0.19–10.3	31–3000	1173–1623
	(0.19–10.3)	(31–3000)	(1173–1923)
MnO	0.04–0.26	31–77	1173–1623
	(0.04–0.40)	(31–3000)	(1173–1923)
MgO	0.05–14.9	31–1513	1173–1837
	(0.05–37.3)	(31–4000)	(1173–2003)
CaO	0.25–29.1	31–4000	1173–1853
	(0.25–48.3)	(31–4000)	(1173–2063)
Na_2O	1.89–13.7	31–4000	1173–1853
	(1.89–21.5)	(31–4000)	(1173–2023)
K_2O	0.14–6.85	31–1513	1173–1813
	(0.14–16.9)	(31–4000)	(1173–1973)

Note: For each oxide the abundance, pressure, and temperature range covered by a minimum frequency of 0.05 of group 1 data in the database is indicated. Numbers in parentheses indicate for each oxide the total range of abundance, pressure, and temperature.

which are high-quality group 1 data produced after 1980. The fraction of data made on natural compositions is 0.41, which increases to 0.71 as long as only the group 1 data are considered. Appendix Table 2 reports the results of a *P*-*T*-composition distribution analysis of the database, which are needed to define the field of calibration of the model. For each oxide, the total range of abundance, pressure, and temperature in the database is reported (in parenthesis) in the table, as well as the range covered by a minimum frequency of 0.05 (corresponding to about 15 experimental constraints) obtained by evaluating only the group 1 data in the database. To assign such frequencies, the total ranges pertaining to each oxide have been divided into 5 classes that are equally spaced for oxide abundance and temperature, and equally spaced on a log-scale for pressure. As an example, consider the case of MgO. The numbers in the table indicate that such an oxide is present in the database with a compositional range from 0.05 to 37.3 wt%, and at pressure and temperature conditions from 31 to 4000 MPa and 1173 to 2003 K, respectively. If we look at only the group 1 data (which, as explained in Appendix 1, represent a heavier constraint on the calibration of the model parameters), and consider as a calibration range the range of classes where the frequency of the group 1 data with respect to the total data is at least 0.05, then the calibration range for the MgO-related model parameters is 0.05–14.9 wt%, 31–1513 MPa, and 1173–1837 K.

As in the table, the field of calibration of the CO_2-related model parameters is large. Compositions range from silica-undersaturated to supersaturated liquids, pressure ranges from a few tens to thousands of megapascals, and temperature ranges from $\leq$1200 to 1600–1900 K. This large range of conditions ensures that the calibration is adequate for the objective of the model. As long as the model is applied within the calibration range defined in Appendix Table 2, its theoretical framework allows an interpolation between experimental data points in a *P*-*T*-10 major oxides space. Outside this range, the model predictions fall in the field of extrapolation, and the modeling results are more confident the closer the conditions are to the calibration limits and the larger the calibration range is. For example, use of the model to predict the H_2O-CO_2-liquid equilibrium for an Etnean tholeiite at 400 MPa pressure and 1300 K temperature can be regarded with a certain confidence even if the tholeiite contains up to 4 wt% Fe_2O_3, whereas the results of an application to a nephelinitic liquid with $\leq$5 wt% Al_2O_3, $\geq$5 wt% Fe_2O_3, and $\geq$18 wt% MgO should be viewed with caution.

MANUSCRIPT RECEIVED NOVEMBER 13, 1997
MANUSCRIPT ACCEPTED OCTOBER 10, 1998
PAPER HANDLED BY REBECCA LANGE